Symbiotic versus nonsymbiotic optimization for spatial and temporal degrees of freedom in pair creation

S. Dong,[1,2] J. Unger,[2] J. Bryan,[2] Q. Su,[2] and R. Grobe[2]

[1]*Key Laboratory for Laser Plasmas, School of Physics and Astronomy, Collaborative Innovation Center of IFSA,*
Shanghai Jiao Tong University, Shanghai 200240, China
[2]*Intense Laser Physics Theory Unit and Department of Physics Illinois State University, Normal, Illinois 61790-4560, USA*

The field-induced decay of the quantum vacuum state associated with the creation of electron-positron pairs can be caused independently by either multiphoton transitions or by tunneling processes. The first mechanism is usually induced by appropriate temporal variations of the external field while the second (Schwinger-like) process occurs if a static but spatially dependent electric field is of supercritical strength. The ultimate goal is to construct an optimal space-time profile of an electromagnetic field that can maximize the creation of particle pairs. The simultaneous optimization of parameters that characterize the spatial and temporal features of both fields suggests that the optimal two-field configuration can be remarkably similar to that predicted from two independent optimizations for the spatial and temporal fields separately.

I. INTRODUCTION

The possibility of probing the instability of the quantum electrodynamical vacuum state with external fields has found considerable interest [1,2] as the result of the recent advances in the development of new light sources with unprecedented high intensities [3]. There are two intrinsically different decay mechanisms, by which electron-positron pairs can be created from the vacuum. The first scheme [4,5] requires the field (which can be static) to be extremely large and can be visualized in terms of a tunneling process [6] between energy shifted Dirac states, while the second scheme [7–14] requires the field to be time dependent with a large frequency leading to single- or multiphoton processes.

In view of this interest, several works [15–21] have begun to develop computational optimization techniques to identify an optimal set of parameters for the field that can maximize the final yield of created electron-positron pairs after the interaction. However, most of these investigations were restricted to examine only those fields that were constant in either space or time. This restriction was necessary due to the computational difficulty of simulating the pair-creation process for those external fields that have both a spatial as well as temporal dependence. Each of these investigations also relies on entirely different theoretical approaches and concepts to determine the final yield.

For spatially inhomogeneous but time-independent fields, a steady-state vacuum decay rate can be defined and calculated conveniently using the Hund rule [22–26], which permits us to map the quantum field theoretical problem onto a quantum mechanical scattering problem [27]. Here the total pair-creation rate (or the rate associated with positrons of a given energy range) can be calculated from the quantum mechanical transmission coefficient. A recent work based on an infinite-dimensional optimization [21] has surprisingly

revealed that there exists an optimal spatial shape for the external supercritical potential $V(x)$. In contrast to what one might expect, this optimal spatial profile for the potential turned out not to be an abrupt step, i.e., $V(x) \sim (1-x/|x|)$ (for which the corresponding electric field is actually infinite), but the optimum $V(x)$ takes a nontrivial and nonmonotonic quasioscillatory shape that is finite.

For external fields with temporal inhomogeneity, the pioneering optimization works by Kohlfürst *et al.* [15,16] and Hebenstreit and Fillion-Gourdeau [17] have employed the quantum Vlasov equation [28–34] to determine the final positron yield. This convenient approach, however, cannot be applied if the field also has a spatial dependence. Due to the inherent difficulty of treating the combined action of two fields with controlled spatial *as well as* temporal inhomogeneity, there have been few systematic investigations that explore the *simultaneous* optimization of both the spatial and temporal degrees of freedom.

Therefore, even the most fundamental questions have not been addressed yet. For example, it would be very beneficial to understand if the resulting optimized superposition of both a temporal and spatial field could be approximated independently from two separate optimizations. If possible, this would correspond to a nonsymbiotic optimization of both degrees of freedom. This possibility of an independent optimization would certainly open the door to simplify future calculations to construct optimal space-time field configurations.

On the other hand, it might also turn out that the optimization is fully symbiotic; i.e., the simultaneous action of both degrees of freedom could lead to the existence of new optimal field configurations, that cannot be deduced or even explained from the independent action of the two fields applied separately. While a finding of this symbiotic nature would make further optimization studies more complicated, from a physical point of view it might be also more fascinating

as it would open the door to the exploration of new phenomena that occur only as a result of the interplay of temporally and spatially induced vacuum decay mechanisms.

In this work we report on some systematic steps towards the long-time goal to construct an optimal electromagnetic-field configuration with optimal spatial as well as temporal shapes. In Sec. II we introduce a quantitive measure that can classify the degree of symbiosis for general systems. In Sec. III we illustrate this measure for a simple model system. In Secs. IV and V we examine the field-induced decay of the vacuum and show that—depending on the field configurations—the optima can be symbiotic as well as non-symbiotic. In Sec. VI we provide open questions and an outlook to future studies.

II. SYMBIOTIC VERSUS NONSYMBIOTIC OPTIMIZATION

Let us denote with $F(t, s)$ the objective functional that maps the external time- and space-dependent force into a single number F. This is the number that needs to be maximized [35–42]. In the introductory Sec. III below, F will represent the final displacement of a simple driven oscillator, and in the main sections, Secs. IV and V, F is the final number of created electron-positron pairs after the interaction with the field. The two parameters t and s that characterize the temporal and spatial characteristics of the applied force field need to be determined to maximize F. In order to quantify the principal difference between a nonsymbiotic and symbiotic optimization, we can construct first the Taylor expansion of the objective function $F(t, s)$ around its local or global maximum, denoted by the pair $\{t_{\text{opt}}, s_{\text{opt}}\}$. As we examine critical points that lead to vanishing first-order derivatives, $\partial_t F(t_{\text{opt}}, s_{\text{opt}}) = \partial_s F(t_{\text{opt}}, s_{\text{opt}}) = 0$, the lowest-order terms of the Taylor expansion of F are given by

$$
\begin{aligned}
F(t, s) = {} & F(t_{\text{opt}}, s_{\text{opt}}) + \partial_s \partial_t F(t_{\text{opt}}, s_{\text{opt}})(t - t_{\text{opt}})(s - s_{\text{opt}}) \\
& + \partial_t^2 F(t_{\text{opt}}, s_{\text{opt}})(t - t_{\text{opt}})^2 / 2 \\
& + \partial_s^2 F(t_{\text{opt}}, s_{\text{opt}})(s - s_{\text{opt}})^2 / 2 + \cdots .
\end{aligned}
\tag{2.1}
$$

We exclude here the case of that rather special set of functions, where the second derivatives around the critical points vanish. For this set, the contour lines around the extreme are ellipses, as we consider in this work. For the special case of a nonsymbiotic maximum, the maximum depends on the parameters t_{opt} and s_{opt} in an independent way. That means that if t is varied slightly from its optimal value $t = t_{\text{opt}}$, the corresponding numerical value for s_{opt} that would keep $F(t, s)$ at its maximum should not change here, and vice versa. In this case, this independence is reflected by the vanishment of the mixed derivative $\partial_t \partial_s F(s_{\text{opt}}, t_{\text{opt}})$.

It seems therefore natural to attribute the magnitude of $\partial_t \partial_s F(t_{\text{opt}}, s_{\text{opt}})$ with the degree of symbiosis. However, as this derivative can carry units in general, its numerical value is not universal as it would change under a possible (and arbitrary) multiplicative scaling of the spatial and temporal degrees of freedom, i.e., $t \to \lambda t$ and $s \to \mu s$. In order to compensate for this possibility, we propose in this work to consider the

following unitless index h,

$$
h(t_{\text{opt}}, s_{\text{opt}}) \equiv (\partial_t \partial_s F)^2 / (\partial_t^2 F \partial_s^2 F),
\tag{2.2}
$$

as a possible measure for the symbiosis. This index is closely related to the determinant of the corresponding 2×2 Hessian matrix, that describes the local curvature and allows us to classify a critical point as a maximum, minimum, or saddle point. For example, $h < 1$ corresponds to a positive Hessian determinant. If h is zero and the two degrees of freedom seem to act independently of each other, we would call the optimum nonsymbiotic. As a side issue, we note that for a maximum F, h is generally constrained to the interval $0 \leqslant h \leqslant 1$.

While it is possible to determine h numerically from the computational data $F(t, s)$ around its maximum, the degree of symbiosis manifests itself also directly in the contour lines of $F(t, s)$ in the space spanned by the temporal and spatial parameters t and s. Here the alignment of the corresponding ellipse around the maxima is related to h. One can show that the alignment angle α between the major semiaxis of the ellipse and the t or s axis is given by $\tan(2\alpha) = 2\partial_t \partial_s F / (\partial_s^2 F - \partial_t^2 F)$. This means that a nonsymbiotic maximum ($h = 0$) can be easily recognized by ellipses that are *not* rotated in (t, s) space.

One of the key questions to be addressed below is about the possibility to obtain a quantitative guidance for the parameter range of the optimal pair $\{t_{\text{opt}}, s_{\text{opt}}\}$ from a (usually much easier) examination of two separate subdynamics. The first system is excited by a space-dependent force only leading to a possible approximation for s_{opt}, while an optimization for a purely temporally driven system could provide an estimate for t_{opt}. We will name the parameter pair obtained from these two *independent* optimizations "*i* points," and denote them by $\{t_{\text{opt}}^{\{1,0\}}, s_{\text{opt}}^{\{0,1\}}\}$ for reasons that become clear in Sec. III.

III. HARMONIC OSCILLATOR AS A PROTOTYPE FOR SYMBIOTIC AND NONSYMBIOTIC OPTIMIZATION

In this section we illustrate the properties of symbiotic and nonsymbiotic optima for an almost analytical model system of a free classical particle, where the spatial and temporal degrees of freedom of the external forces are provided by the spatial scale of a harmonic oscillator and by the temporal scale of a monochromatic driving force. As we will show below, in this particular system, the global optimum is nonsymbiotic while the first local optimum is symbiotic. We will illustrate the different graphical implications of contour plots around these two optima and examine the quality of the corresponding *i* points to predict the true optima of the system driven by both forces.

A. Simultaneous optimization and the Hessian index

In order to illustrate the different characteristics of symbiotic versus nonsymbiotic maxima in the space of the temporal and spatial control parameters, we examine here the simplest possible model system, a driven harmonic oscillator of unit mass, given by the Hamilton function

$$
H = P^2 / 2 + B\Omega^2 X^2 / 2 - A \sin(\omega t) X.
\tag{3.1}
$$

Here we have used a unit system for which the mass is equal to 1. Choosing the pair of two parameters $\{A, B\} = \{1, 0\}$ or
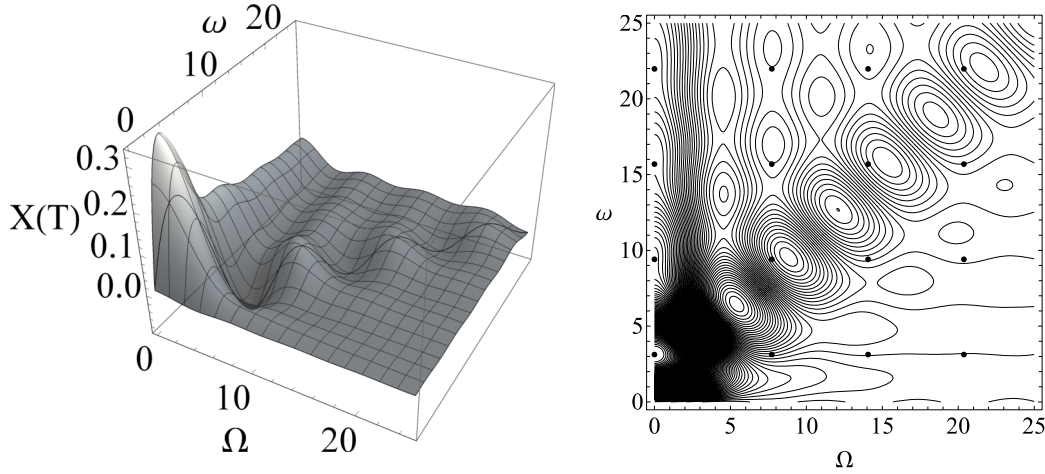
FIG. 1. (left) Surface plot of the final displacement $X(\omega, \Omega)$ for $T = 1$ and $V = 0.01$ For better readability we have also included as a reference line the diagonal $\Omega = \omega$. (right) The corresponding contour lines. The sixteen black dots are the locations of the first 16 i points, discussed in Secs. III B and III C.

{0,1} permits us to examine the temporal and spatial optimization separately from each other, while the notation {1,1} corresponds to the fully coupled dynamics. Let us assume the goal is to find the optimal control pair $\{\omega_{\text{opt}}, \Omega_{\text{opt}}\}$, such that for a given initial condition $X(0) = 0$ and $dX/dt(0) = V$ the displacement from equilibrium at a final interaction time $X(T)$ is maximal.

Due to the simplicity of the {1,1} system, we can solve the corresponding set of Hamilton equations analytically and obtain for the final displacement at time T

$$X(\omega, \Omega) = \{\Omega \sin(\omega T) - [\omega - V(\omega^2 - \Omega^2)] \sin(\Omega T)\} \Omega^{-1}$$
$$\times (\Omega^2 - \omega^2)^{-1}. \tag{3.2}$$

The necessary condition for any critical points, i.e., $\partial X/\partial \omega = \partial X/\partial \Omega = 0$, is unfortunately a transcendental coupled set of equations and therefore needs to be solved numerically.

To get a qualitative picture first, we have graphed in Fig. 1 the corresponding surface plot for $X(\omega, \Omega)$ as a function of the two control parameters ω and Ω, together with the corresponding contour plot. As the two parameters in the coordinate pair (Ω, ω) are independent of each other, we have chosen in our graphs an arrangement of the two coordinate axes that is similar to the usual matrix notation, where the first component is the vertical location (column) and the second component denotes the horizontal location (row) within the matrix.

We see that the global maximum occurs for the pair $\{\omega_{\text{opt}}, \Omega_{\text{opt}}\} = \{\pi/T, 0\}$. This set of control parameters makes sense as the choice $\Omega_{\text{opt}} = 0$ removes the effect of the spatial force entirely, which due to its binding character would oppose any large displacements $X(T)$. The numerical value for the optimal temporal control parameter $\omega_{\text{opt}} = \pi/T$ is also expected, as with this particular choice the particle can experience the first full half cycle of the oscillating field, which can therefore maximally accelerate the particle to a larger position, before the force direction would reverse itself for $t > T$. The Hessian index h for the global maximum is exactly zero here, consistent with the observed vanishing angle between the semiaxes and the t and s coordinate axes.

The global maximum is therefore fully nonsymbiotic in this system.

On the other hand, the first local maximum is calculated to be at $\{\omega_{\text{opt}}, \Omega_{\text{opt}}\} = \{9.560, 8.816\}$. Its Hessian index is determined as $h = 0.222$ and (for normalized axes and a unit aspect ratio) the corresponding angle of the semimajor (or -minor) axis is $\alpha = -42.9°$. Therefore, the first local maximum happens to be symbiotic, which is consistent with the rotated ellipses in the contour plot.

B. Mathematical i points obtained from independent optimizations

The key question, of course, is whether it is possible to obtain an estimate of the locations of the numerical values for $\{\omega_{\text{opt}}, \Omega_{\text{opt}}\}$ from independent (and for more complicated systems computationally significantly easier) calculations, where *either* solely the spatial *or* the temporal forces are acting. As we have discussed in the Introduction, the example of the vacuum decay shows that when particles are created by either solely temporal or spatial force fields, the computational analysis is much easier.

For the (solely) temporal system $\{A, B\} = \{1, 0\}$, given by the Hamiltonian $H = P^2/2 - \sin(\omega t)X$, the final displacement is $X(\omega, 0) = T/\omega + VT - (1/\omega^2)\sin(\omega T)$, consistent with the limit of $X(\omega, \Omega \to 0)$ of Eq. (3.2). As the initial velocity V enters the solution only via an additive term, it does not impact the location of the maxima. For $T = 1$ the first four maxima for $X(T)$ occur at $\omega_{\text{opt}}^{\{1,0\}} = 3.142, 9.425, 15.708$, and 21.81 [associated with decreasing magnitudes for $X(\omega_{\text{opt}}, 0)$].

Similarly, the spatially only forced system (corresponding to $\{A, B\} = \{0, 1\}$) is given by $H = P^2/2 + \Omega^2 X^2/2$, leading to $X(0, \Omega) = V\sin(\Omega T)/\Omega$. The values for the optimal spatial scales can be found numerically as $\Omega_{\text{opt}}^{\{0,1\}} = 0, 7.725, 14.07$, and 20.371. Also, these values do not depend on the initial velocity V of the particle.

Even though the {1,0} and the {0,1} systems are completely different physical systems and do not have anything in common, we can (purely mathematically) combine their optima to pairs, denoted by $\{\omega_{\text{opt}}^{\{1,0\}}, \Omega_{\text{opt}}^{\{0,1\}}\}$. More

specifically, if we focus on the first four optima of each set, we obtain a total of 16 "coordinate pairs" denoted by $i_{m,n} \equiv \{\omega_{\mathrm{opt},(m)}^{\{1,0\}}, \Omega_{\mathrm{opt},(n)}^{\{0,1\}}\}$ with $m = 1, 2, 3, 4$ and $n = 1, 2, 3, 4$. To reflect the complete independence of the first and second coordinate in each pair, we denote them as "independent points," or i points. We stress here that any pair $\{\omega_{\mathrm{opt}}^{\{1,0\}}, \Omega_{\mathrm{opt}}^{\{0,1\}}\}$ cannot be associated with any single physical system.

In the contour plot of the physical system (for $\{A = 1, B = 1\}$) shown in Fig. 1 above, we have added the locations of these 16 i points $i_{m,n}$. Quite remarkably, we find that some of them ($i_{m,n}$ with $n = 1$) match exactly the locations of the true optima, while others ($i_{m,n}$ with $m > n$) seem to be located remarkably close to a true optimum. The exact match of the i points $i_{m,n}$ with $n = 1$ is expected as the subsystem $\{A = 1, B = 0\}$ is—by definition—identical to the full system $\{A = 1, B = 1\}$ if $\Omega = 0$. We remind the reader that all of these four maxima also had vanishing Hessian indices $h = 0$. As some of the true optima are associated with $\Omega = 0$, the corresponding exact match with the i points is therefore obvious.

On the other hand, quite remarkably, other i points apparently can also serve as good guidance to find the actual locations of the true optima. To be more specific and provide a qualitative example, the three i points $\{\omega_{\mathrm{opt}}^{\{1,0\}}, \Omega_{\mathrm{opt}}^{\{0,1\}}\}$, given by $i_{2,2} = \{9.425, 7.725\}$, $i_{3,3} = \{15.71, 14.07\}$, and $i_{4,4} = \{21.81, 20.371\}$ are in the direct vicinity of the locations of the true optima, which are located at $\{9.560, 8.816\}$, $\{15.808, 15.3125\}$, and $\{22.0747, 21.6859\}$.

C. Back tracing of i points to true optima

As we have seen above, the numerical data seem to suggest the set of i points can indeed serve as qualitative guidance to predict the locations of the fully space-time forced $\{A = 1, B = 1\}$ system. However, in order to exclude the possibility that this qualitative matching is just purely accidental, and to establish an unambiguous one-to-one connection between a true optimum and the corresponding mathematical i point, it would be desirable to establish some kind of direct link between them.

This task is not so trivial as the i points are merely mathematical constructs, whose coordinates were artificially patched together from two completely independent systems $\{A = 1, B = 0\}$ and $\{A = 0, B = 1\}$. However, if we introduce a running constant denoted by ε, whose value is increased from $\varepsilon = 0$ to $\varepsilon = 1$, we could examine the resulting continuous pathway that the corresponding i points $\{\omega_{\mathrm{opt}}^{\{1,\varepsilon\}}, \Omega_{\mathrm{opt}}^{\{\varepsilon,1\}}\}$ would take as a function of ε. More specifically, for the system $\{A = 1, B = \varepsilon\}$ we would obtain an equation for the pair $\{\omega, \Omega\}$ that fulfills $\partial X^{\{1,\varepsilon\}}/\partial\omega = 0$ and similarly, for the system $\{A = \varepsilon, B = 1\}$ we obtain a second equation $\partial X^{\{\varepsilon,1\}}/\partial\Omega = 0$. If we then (artificially) require to solve these two equations together, we obtain the corresponding i point, denoted by point $\{\omega_{\mathrm{opt}}^{\{1,\varepsilon\}}, \Omega_{\mathrm{opt}}^{\{\varepsilon,1\}}\}$. While we stress again that for each value of ε (not equal to 1) the sequence of i points does not correspond to any single physical system, for $\varepsilon = 1$ they do describe the system $\{A = 1, B = 1\}$. In other words, in this way we have managed to construct a *continuous* connection between the i point and the physical system of interest. The
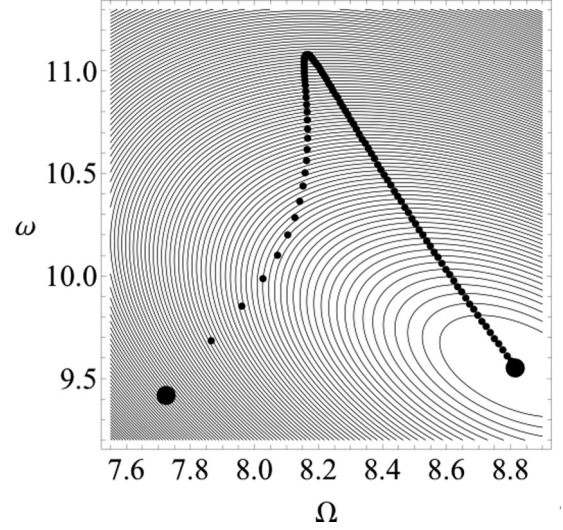

FIG. 2. The connection pathway between the i point $i_{2,2} = \{\omega, \Omega\} = \{9.425, 7.725\}$ and the true optimum for the $\{A = 1, B = 1\}$ space-time forced system given by $\{9.560, 8.816\}$. The pathway was linearly parametrized as a function of ε as $\{\omega_{\mathrm{opt}}^{\{1,\varepsilon\}}, \Omega_{\mathrm{opt}}^{\{\varepsilon,1\}}\}$ with $0 \leqslant \varepsilon \leqslant 1$.

most important question, of course, is to find out which of the maxima each i point can be linked to by this particular scheme.

We have numerically examined this question and found that the specific points $i_{m,1}$ consistently do not depend on ε, while the other points (for $m > n$) evolve indeed to their nearest true maximum. This means that it is indeed unambiguously possible to uniquely connect some i points to their "parent" value (given by the coordinate pair of the true maximum).

As a side issue, we should mention that these pathways are usually not straight lines and sometimes even move away first from the true maximum before they return. In fact, the details of the pathway do depend on the way the two coefficients A and B are parametrized by ε. However, we found that the endpoints (for $\varepsilon = 1$) for unique and differently parametrized paths always moved to exactly the same location. In Fig. 2 we have shown an example for these connection pathways. It shows how the i point $i_{2,2}$ (given by $\{9.425, 7.725\}$) evolves to the true optimum $\{9.560, 8.816\}$ for the simplest (linear) parametrization given by $\{A = 1, B = \varepsilon\}$ and $\{A = \varepsilon, B = 1\}$.

D. Orphan i points that cannot be traced back to true optima

If we examine those i points in Fig. 1 that are below the $\omega = \Omega$ diagonal (i.e., $\omega < \Omega$), we find that the association between each i point $\{\omega_{\mathrm{opt}}^{\{1,0\}}, \Omega_{\mathrm{opt}}^{\{0,1\}}\}$ and its corresponding parent parameters (given by the true optimum $\{\omega_{\mathrm{opt}}^{\{1,1\}}, \Omega_{\mathrm{opt}}^{\{1,1\}}\}$) is no longer obvious or sometimes not even possible. In fact, we will illustrate below that some i points can no longer be traced back to any optimum. We would denote these particular isolated i points that are not so useful in finding the true optima as "orphan" i points.

As a concrete illustration of how an i point can become an orphan and how this transition manifests itself in a rapidly rising Hessian index of the true optimum, we examine here

as a concrete example the fate of the i point given by the "coordinates" $i_{2,3} = \{9.425, 14.07\}$. Even though there is a (very shallow) maximum for $V = 0.1$ (see Fig. 1) nearby, it turns out that this point is not the parent maximum to this particular i point.

As we noted above, in contrast to the location of the true optimum, these two coordinates are independent of the initial velocity V. However, the very existence as well as the location of the true optima do depend on the velocity. The contour plot for $V = 0.01$ (see Fig. 1) showed that there seemed to be no optimum that could be easily assigned to $i_{2,3}$. It turns out that for $V = 0.01$ there is actually no associated optimum and therefore $i_{2,3}$ is an example of an orphan point.

To prove this feature of $i_{2,3}$, we show that for $V > 0.0903$ the corresponding maximum can actually be recovered. Using the backtracing technique discussed in Sec. III C for $V > 0.0903$, one can construct a direct pathway from $i_{2,3}$ to the maximum. For example, for $V = 0.12$ this maximum is located at $\{7.84, 13.90\}$.

In Fig. 3 we illustrate graphically how a maximum can actually disappear if the velocity is decreased beyond $V = 0.0903$. As shown in the contour plot of $X(\omega, \Omega)$ for $V = 0.12$, in the immediate vicinity of the maximum at $\{7.84, 13.90\}$ there is also a saddle point centered at $\{8.02, 12.59\}$. As the velocity is decreased, these two critical points approach each other with the result that at $V = 0.0903$ the two points match and the saddle point eradicates the maximum. At the same time, our i point $i_{2,3}$ becomes an orphan as it can no longer be traced back to any (parent) optimum of the physical system. The "orbits" of the two critical points with decreasing V in the $\{\omega, \Omega\}$ plane are also depicted in Fig. 3(b). Consistent with the definition of the Hessian index, h also increases from basically zero (for $V > 0.1$) to $h = 1$ (for $V < 0.0903$), which is characteristic of a saddle point. In Fig. 3(a) we have graphed the rapid rise of h with decreasing velocity V.

As a side issue, we should point out that this saddle point has an unusually asymmetric feature. The final displacement $X(T)$ decreases along the positive and negative ω direction as well as the positive Ω direction, but it increases only along the negative Ω direction. For an even smaller velocity $V < 0.088$, even this saddle point ceases to exist, completing the transition from originally two to one and finally zero critical points as the velocity decreases.

E. Final displacement at the maxima

So far our focus was entirely on the location of the optimal parameters $\{\omega_{\text{opt}}, \Omega_{\text{opt}}\}$ in the two-dimensional control space, their relationship to the true optima, the orientation of the ellipses around the maxima, and their h indices. It might also be interesting to examine the actual values of the optimum displacement X and to compare their magnitudes with those obtained from the two subsystems $\{A = 1, B = 0\}$ and $\{A = 0, B = 1\}$. We could then examine whether a large h index corresponds to those cases where the final displacement $X^{\{1,1\}}$ of the combined action of both forces is actually much larger than the displacements $X^{\{1,0\}}$ or $X^{\{0,1\}}$.

Our numerical data suggest that this is actually not the case at all for our particular system; it almost seems that the temporal and spatial excitation mechanisms are here in direct
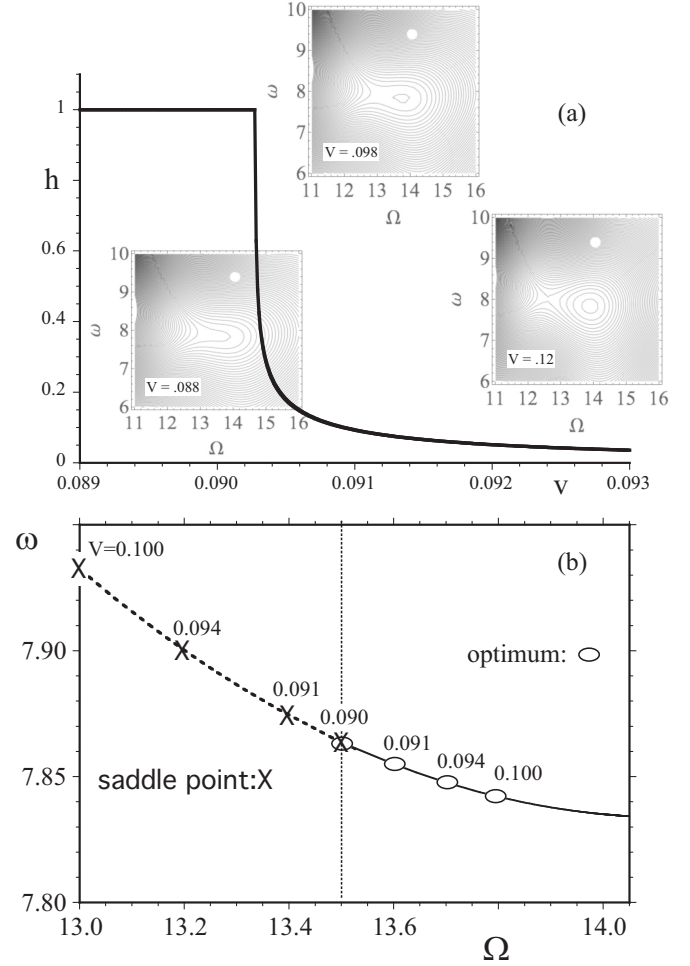

FIG. 3. The disappearance of optima for the system with decreasing initial velocity V. (a) The Hessian index h as an indicator of the transition from a maximum ($h < 1$) to a saddle point ($h = 1$) as a function of V. The three insets show the corresponding contour plots of $X(\omega, \Omega)$ for three different values of the velocity. For reference, the white dot is the i point, $i_{2,3} = \{9.425, 14.07\}$, whose coordinates are independent of the velocity. (b) The orbits of the center of the ellipse and the saddle point in the $\{\omega, \Omega\}$ plane with decreasing velocity.

competition with each other. We have not encountered a single local maximum where $X^{\{1,1\}}$ was actually larger compared to either $X^{\{1,0\}}$ or $X^{\{0,1\}}$, evaluated at the i points. For example, for the first local maximum associated with the i point $i_{2,2}$ we find that the corresponding amplification factor, defined as $X^{\{1,1\}}/\max[X^{\{1,0\}}, X^{\{0,1\}}]$ is only 0.48. This ratio is even further decreasing from 0.44 (for $i_{3,3}$) to 0.42 (for $i_{4,4}$).

This—at first unexpected—attenuation turns out to be a direct consequence of the drift associated with the specific initial turn-on phase of the temporal driving force. For the Hamiltonian of the $\{1,0\}$ system, i.e., $H = P^2/2 - \sin(\omega t)X$, the time-dependent solution $X(t) = t/\omega - \sin(\omega t)/\omega^2$ reveals this drift term t/ω. As a comparison, this large term is even double the size of the largest position of the harmonic oscillator at full resonance, i.e., $H = P^2/2 - \sin(\omega t)X + \omega^2 X^2/2$, which takes the solution $X(t) = -t/(2\omega)\cos(\omega t) + \sin(\omega t)/(2\omega^2)$. For large and optimal times, we would therefore find that the amplification ratio is only $X^{\{1,1\}}/\max[X^{\{1,0\}}, X^{\{0,1\}}] \approx$

$(t/\omega)/[t/(2\omega)] = 0.5$, which is fully consistent with the numerical values found above. This illustrates analytically that in this system, the presence of the binding potential $\omega^2 X^2/2$, in the {1,1} system, cannot act as a true amplifying agent for $X(t)$.

Had we chosen a different turn-on phase of the force in the {1,0} system, such as $H = P^2/2 - \cos(\omega t)X$, then the solution $X(t) = [1 - \cos(\omega t)]/\omega^2$ would be only purely oscillatory and would not contain any drift term. In this case, the maximum position of the corresponding {1,1} system, i.e., $H = P^2/2 - \cos(\omega t)X + \omega^2 X^2/2$, is then given by $X(t) = t/(2\omega)\sin(\omega t)$. This means that here the amplification factor $X^{\{1,1\}}/\max[X^{\{1,0\}}, X^{\{0,1\}}]$ would actually grow linearly in time, reflecting a much more constructive collaborative action of the temporal and spatial forces. Quite remarkably, for any finite interaction time T, the global maximum for this particular system is at $\{\omega_{\text{opt}}, \Omega_{\text{opt}}\} = \{0, 0\}$ with the optimum value $X(T) = T^2/2$, reflecting once again that—even for this turn-on phase—the absence of any binding potential is still preferred to optimize a final position of a particle, despite the possibility of a resonance.

IV. ELECTRON-POSITRON PAIR CREATION DUE TO EITHER TEMPORAL OR SPATIAL EXCITATIONS

In this section, we apply the derived i-point method to identify the possible location of two control parameters that optimize a physical process to the quantum field theoretical dynamics of electron-positron pair creation. We will briefly summarize the methodology of computational quantum field theory to calculate the vacuum decay process and to determine the final number of created electron-positron pairs at a given energy. While some of the prior optimization studies of solely temporal [20] or spatial fields [21] could be accomplished based on infinite-dimensional optimization, to get some insight into combined space-time optimization processes, we begin with only a finite-dimensional optimization based on only two control parameters [15–17,19]. The time-dependent electric field is characterized by a varying frequency ω, while for the spatially inhomogeneous field we have varied either the spatial extension W or the amplitude V_b. In each of the three (separate) cases we have found a regime in which a finite parameter can lead to one or several maxima with regard to the final number of created electron-positron pairs after the interaction. The key idea in this section will be to illustrate that the i-point methodology can even be generalized from classical mechanical systems to predict quantum field theoretical dynamics.

A. Computational quantum field theoretical description

Let us first briefly summarize our quantum field theoretical system to describe the vacuum decay process. It is based on the numerical solutions of the electron-positron field operator from the time-dependent Dirac equation, $i\hbar\partial\Psi/\partial t = H\Psi$. In one spatial dimension (and atomic units, where $m = 1$, $q = -1$, $\hbar = 1$, and $c = 137.036$), the Hamiltonian takes the following form:

$$H = c\sigma_1 p_x + \sigma_1 A(x, t) + c^2\sigma_3 - V(x)\sigma_0, \quad (4.1)$$

where σ_i (with $i = 0, 1, 2, 3$) denotes the set of the four 2×2 Pauli matrices that satisfy the anticommutation relations $\{\sigma_i, \sigma_j\} = 2\delta_{i,j}$. The spatially induced (supercritical) part of the external force field is modeled by a (supercritical) potential step $V(x)$ with a controlled spatial inhomogeneity. The associated electric-field points along the x direction and is spatially localized along the x direction. The temporal part with a controlled time dependence is modeled by a vector potential $A(x, t)$, whose spatial profile was chosen to guarantee that the temporally induced pair creation occurs only in the finite region in space, where $V'(x)$ does not vanish.

The initial vacuum state is represented by the set of occupied eigenstates $|k; d\rangle$ of the (field-free) Dirac operator $H_0[=c\sigma_1 p_x + c^2\sigma_3]$ with negative energy that satisfy $H_0|k; d\rangle = -[c^4 + c^2 k^2]^{1/2}|k; d\rangle$. We assume that our system has a finite spatial extension L and that all states satisfy periodic boundary conditions. As a result, the states can be normalized as $\langle k_1; d|k_2; d\rangle = \delta_{k1,k2}$ and they have a momentum mode spacing $\Delta k = 2\pi/L$. The corresponding positive-energy states with momentum p are denoted by $|p; u\rangle$. In computational quantum field theory [43] the required space-time evolution of the electron-positron quantum field operator can be obtained equivalently from the time evolution of the set of all states $|k; d\rangle$ and the resulting matrix elements $U_{pk}(t) \equiv \langle p; u|U(t)|k; d\rangle$, where $U(t)$ is the time-ordered evolution operator associated with H. The solutions of the space-time-dependent Dirac equation with the external potentials $A(x, t)$ and $V(x)$ can be obtained on a space-time lattice with N_t temporal and N_x spatial grid points using efficient fast-Fourier transformation based split-operator schemes [44–46]. The main quantity of interest in this work, the total number of created electron-positron pairs after the interaction at final time T, is then obtained from all time-evolved Hilbert-space states as $N(T) \equiv \Sigma_{p,k}|U_{pk}(t)|^2$.

In order to make our numerical simulations less CPU time consuming, in this work we represent the vacuum by just a single initial state, which is equivalent to focusing on the creation of an electron with a specific final energy E only. In this work we have chosen $E = 1.25c^2$ corresponding to an initial state with negative energy $-1.25c^2$ of the positronic Dirac sea.

B. Optimal frequencies of the temporal force only

The temporal vector potential $A(t)$ is mainly characterized by its frequency ω, the amplitude F_0 of the associated electric field, and an overall (super-Gaussian) envelope that guarantees a smooth turn-on and -off. The temporal turn-off was chosen to remove any ambiguity in the interpretation of $N(T)$ to represent either a real or quasiparticle pair [33,47]. In order to restrict the temporal pair creation to the same spatial region where the spatially induced pair creation occurs [see Eqs. (4.3) and (4.4) below], we have chosen $A(t)$ to be nonzero only to the region where $V'(x)$ is mainly nonzero.

$$A(t) = F_0 c/\omega \exp[-(t - T/2)^4/(0.02T^4)]\cos(\omega t). \quad (4.2)$$

In our numerical simulations we fixed the amplitude of the electric field to $F_0 = 0.3c^3$. As a temporal control parameter, we have varied the oscillation frequency ω of the vector potential.
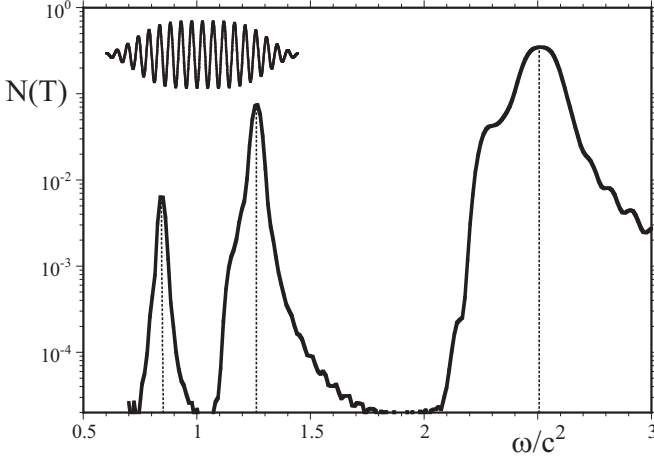
FIG. 4. The final number $N(T)$ of created electron-positron pairs after the interaction of the vacuum state as a function of the frequency ω of a time-dependent electric field given by the vector potential $A(t) = F_0 c/\omega \exp[-(t-T/2)^4/(0.02T^4)]\cos(\omega t)$, shown in the inset for $\omega = c^2$. For reference the three dashed vertical lines point to $\omega_{\text{opt}}^{\{1,0\}} = 0.844$, 1.26, and 2.51. ($F_0 = 0.3c^3$, $T = 0.006$ a.u., $L = 1.5$ a.u., the electric field was chosen to be nonzero for a spatial region of length $L/4$, $N_x = 4096$, $N_t = 6000$).

In Fig. 4 we show the final number of created positrons $N(T)$ after the interaction with the pulse as a function of the oscillation frequency ω of the field. As expected, the global maximum occurs for $\omega = 2.51c^2$ as this particular frequency matches roughly the energy difference of the initial state (at energy $E = -1.25c^2$) and that of the most likely coupled state in the positive energy continuum (with $E = 1.25c^2$). However, if this energy difference can be matched with any integer multiple of the external frequency, we have additional maxima. The first two of them are shown in Fig. 4 by the dashed lines and correspond to $\omega = 1.26c^2$ and $\omega = 0.844c^2$, which can be loosely interpreted as the result of the absorption process of two and three photons. As the three frequencies that couple the initial states to the continuum states are actually remarkably close to the values given by $\omega = 2E/n$ for $n = 1$, 2, and 3, the field-induced level shift as well as finite pulse effects are not so important for this choice of the field amplitude F_0. In fact, we are here still in the perturbative regime, where the peak heights $N(t)$ scale linearly, quadratically, and cubically with the field intensity F_0^2.

C. Optimal width of the spatial force

In order to establish the steady state of the pair creation due to a temporally inhomogeneous electric field, the corresponding potential $V(x)$ must be supercritical, i.e., the difference $|V(x \to -\infty) - V(x \to \infty)| > 2c^2$. To have a simple case, for which the pair-creation rate in the steady state can also be obtained analytically, we have examined here a smooth potential step given by the form $V(x) = V_0[1-\tanh(x/W)]/2$, where W denotes the width. Except for the data presented below in Fig. 5, we have fixed the value of V_0 to $2.5c^2$ to guarantee supercriticality. For this case, the pair-creation rate per unit energy can be found based on a transmission coefficient $\tau(E)$,
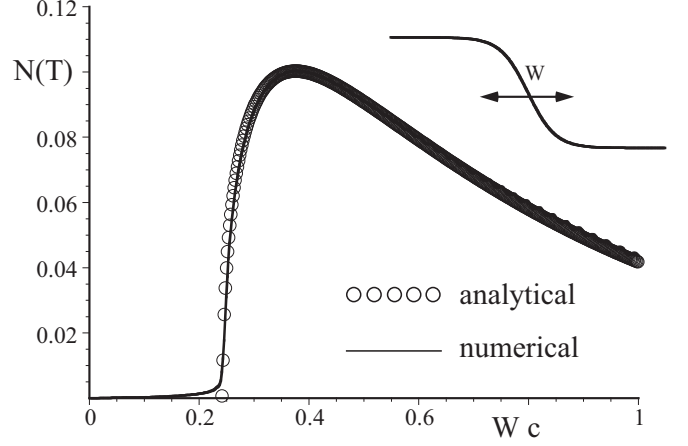

FIG. 5. The final number $N(T)$ of created electron-positron pairs after the interaction of the vacuum state as a function of the spatial extension W of the electric field $E(t) = -dV/dx$, where $V(x) = V_0[1-\tanh(x/W)]/2$ and $V_0 = 2.5c^2(Wc/0.3)^{1/2}$, as shown in the inset. The analytical predictions are based on the steady-state decay rate given by Eq. (4.3). ($T = 0.006$ a.u.; $V(x)$ was turned on smoothly in time over 0.0002 a.u.).

which is given by an analytical expression [46,48,49],

$$\tau(E) = -\sinh[\pi p W]\sinh[\pi k W]/$$
$$\{\sinh[\pi(|V_0|/c + p + k)W/2]$$
$$\times \sinh[p(|V_0|/c - p - k)W/2]\}, \qquad (4.3)$$

where the two momenta are given by $k = -[(E-|V_0|)^2-c^4]^{1/2}/c$ and $p = [E^2-c^4]^{1/2}/c$. It was shown in Ref. [27] that this transmission coefficient $\tau(E)$ can be used to construct the number density of created positrons at final time T for a given energy E via $N_{\text{analyt}}(T) = 1/L\tau(E)v_{\text{inc}}T$, where L is the extension of the numerical box and v_{inc} the velocity of the (incoming) negaton state that populates the final positron state with energy E.

As $\tau(E)$ in Eq. (4.3) decreases monotonically with increasing width W, the true optimum width would be zero, corresponding to an abrupt potential step $V(x) = V_0(1-x/|x|)/2$. In order to study a situation where we have a well-defined maximum that is not located at a boundary, we have constrained the resulting "energy" of the corresponding electric field $-dV/dx$ to satisfy $\int dx(dV/dx)^2 = $ constant. This requirement leads to a width-dependent potential strength $V_0 = 2.5c^2(Wc/0.3)^{1/2}$. The numerical value 0.3 was chosen arbitrarily, such that for $W = 0.3/c$ we obtain $V_0 = 2.5c^2$. It is clear that as a consequence of this particular choice the potential is supercritical only if $V_0 > 2c^2$, i.e., $2.5c^2(Wc/0.3)^{1/2} > 2c^2$. This means that positrons can only be created if the width fulfills $W > 0.192/c$. While in the opposite limit, $W \to \infty$, the extension of the corresponding electric field is infinite, the maximum amplitude of the electric field approaches zero, i.e., $-dV/dx|_{x=0} \to -1.14c^{5/2}W^{-1/2}$. This means that for both limits $W > 0.192/c$ and $W \to \infty$ the positron creation rate vanishes and we expect a maximum in between. By equating the derivative of $\tau(E)$ to zero, we find that the optimum width for $E = 1.25c^2$ occurs at $W_{\text{opt}} = 0.375/c$.
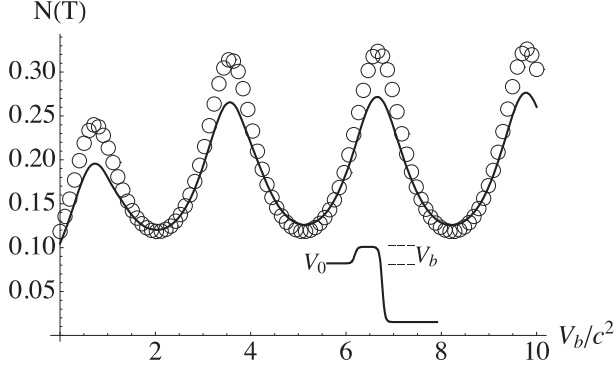
FIG. 6. The final number $N(T)$ of created electron-positron pairs after the interaction of the vacuum state as a function of amplitude V_b of the bump. Here $V(x)$ corresponds to a smooth two-step potential as described in the text and shown in the inset. The open circles are the approximate and rate-based predictions according to the analytical expression Eq. (4.5) ($V_0 = 2.5c^2$, $T = 0.006$ a.u.; the potential was turned on smoothly over a time 0.0001 a.u.).

In Fig. 5 we show the (rate-based) analytical prediction for $N(T)$ according to Eq. (4.3) together with the numerically obtained number of positrons after the interaction time $T = 0.006$ a.u. The agreement is very good, which suggests that this interaction time was sufficiently long such that the transient temporal turn-on effects associated with finite times are not so important.

D. Optimal amplitudes for the spatial force only

As a complementary way to control the spatial potential $V(x)$, we have also varied the amplitude V_b of an additional bump of width d that has been placed on top of the Sauter potential discussed in Sec. IV C. The reason for this particular choice for $V(x)$ is twofold. First, $V(x)$ mimics the actual spatial shape of *the* optimal potential rather well which can be obtained numerically via an infinite-dimensional optimization scheme [21]. Second, due to its simple functional form, one can even obtain here also an approximate (but analytical) form of the steady-state pair-creation rate. The functional form of this potential is given by

$$V(x) = V_0[1 - \tanh(x/w)]/2 + V_b\{\tanh[(x + d)/w] - \tanh(x/w)\}/2, \quad (4.4)$$

where we keep the amplitude $V_0 = 2.5c^2$, the width $w = 0.1/c$, and the size $d = 1/c$ constant. In the inset of Fig. 6 we show the spatial form of this potential $V(x)$. For similar parameters as in Fig. 5 we display also here the final number of created positrons $N(T)$ after the interaction with this supercritical potential as a function of the magnitude V_b of the additional bump.

The sequence of maxima and minima are associated with a resonant match between the wavelength of the corresponding negative energy states under the spatial extension d of the bump. More details are discussed in Ref. [21]. Similar to the potential discussed in Sec. IV C, the data for $N(T)$ can also here be approximated by an analytical expression. If we assume that the spatial width w is equal to zero, then the supercritical scalar potential is characterized by two abrupt

steps, given by $V(x) \equiv V_0$ for $x < -d$, $V(x) \equiv V_0 + V_b$ for $-d < x < 0$, and $V(x) \equiv 0$ for $0 < x$. Due to its simple functional form, one can construct analytically the corresponding stationary energy eigenstate for a positive energy E by matching the analytical solution at the boundaries at $x = -d$ and $x = 0$ based on the continuity equation. The resulting analytical expression for the transmission coefficient is derived in Ref. [50] as $\tau(E) = 4c^4pq_0q_1^2/(N_1 + N_2)$, where

$$N_1 \equiv c^2q_1^2[(E-c^2)^{1/2}(E_0-c^2)^{1/2} + (E + c^2)^{1/2}(E_0 + c^2)^{1/2} + c^2]^2\cos^2(q_1d), \quad (4.5a)$$

$$N_2 \equiv \{E_1[(E + c^2)^{1/2}(E_0-c^2)^{1/2} + (E-c^2)^{1/2}(E_0 + c^2)^{1/2} + c^2] + c^2[(E + c^2)^{1/2}(E_0-c^2)^{1/2} - (E-c^2)^{1/2}(E_0 + c^2)^{1/2}]\}^2\sin^2(q_1d), \quad (4.5b)$$

and where the three momenta are $p(E) \equiv (E^2-c^4)^{1/2}/c$, $q_1(E) \equiv [(V_b + V_0-E)^2-c^4]^{1/2}/c$, and $q_0(E) \equiv [(V_0-E)^2 - c^4]^{1/2}/c$, and the relevant shifted energies are $E_0 \equiv V_0-E$ and $E_1 \equiv V_b + V_0-E$.

As discussed above we can approximate here again the final number of created positrons at energy E via $N_{\text{analyt}}(T) = 1/L\tau(E)v_{\text{inc}}T$, which are indicated by the circles in Fig. 6. The differences between both sets of data are associated with the nonzero width w of the exact data as well as the early-time transients that are unavoidably associated with any temporally turned-on force fields. As $N(T)$ uniformly decreases with increasing width w, the analytical data (based on $w = 0$) should overestimate the true number of created positrons.

In order to separate the transient effects from those associated with a nonzero width w, we have repeated the numerical simulations for the potential with $w = 0$. In order to appropriately sample the corresponding abrupt changes of $V(x)$ at $x = -d$ and $x = 0$, this required an extremely large number of spatial grid points to obtain numerically converged results. We found that here the data up to $V_b < 10c^2$ were graphically indistinguishable from the analytical data predicted by Eqs. (4.5a) and (4.5b). Depending on whether $N(t)$ after the early-time transient period rose above or below the analytical prediction [based on the constant growth rate $1/L\tau(E)v_{\text{inc}}$], the final number of created positrons was either under- or overestimated by the analytical form at the end of the interaction.

As suggested by the data in Fig. 6, the locations of the maxima are remarkably well approximated by the analytical expression. The exact values for the first three maxima, given by $V_b/c^2 = \{0.733, 3.56, 6.66\}$, differ only insignificantly from the analytical ones, which can be derived as $V_b/c^2 = \{0.731, 3.57, 6.67\}$.

V. ELECTRON-POSITRON PAIR CREATION DUE TO SIMULTANEOUS TEMPORAL AND SPATIAL EXCITATIONS

Now that the i points are well defined through the two decoupled single-parameter dynamics, in this section we will examine the combined action of space- and time-dependent
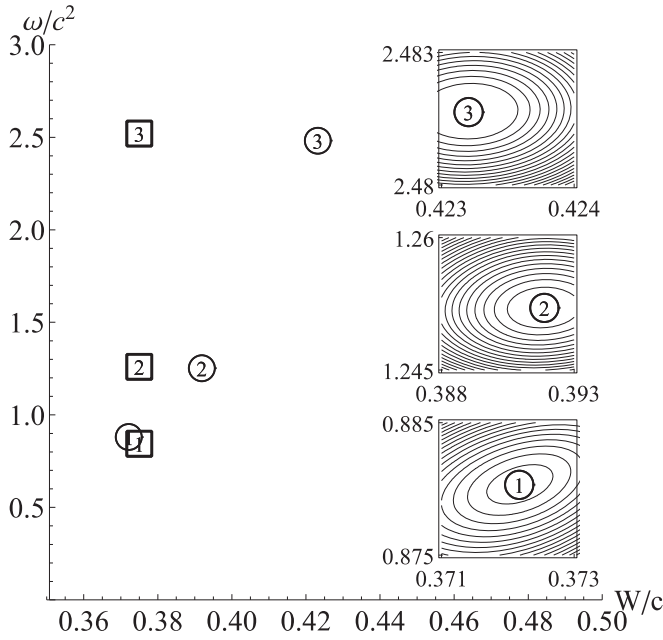
FIG. 7. The locations of the true optima (open circles) and the corresponding i points (open squares) for $N(T)$ in the (ω, W) plane. In the inset we show the corresponding contour plots around the true optima. The i points are located at $i_1 = \{\omega/c^2, Wc\} = \{0.844, 0.375\}$, $i_2 = \{1.26, 0.375\}$, $i_3 = \{2.52, 0.375\}$, and the corresponding true optima are at $\{0.880, 0.372\}$, $\{1.25, 0.392\}$, and $\{2.48, 0.423\}$. ($F_0 = 0.3c^3$, $V_0 = 2.5c^2$, $T = 0.006$ a.u.; the potential $V(x)$ was turned on smoothly over a time 0.0001 a.u.).

force fields. We illustrate here for a concrete set of parameters that the i-point methodology can guide us to narrow down the search space for optimal parameters. The key point will be the observation that the approach from the simple model system in Sec. III concerning the usefulness of the i points as well as the Hessian index and its graphical manifestation can indeed be generalized to this much more complicated quantum field theoretical system. For the temporal system, we have seen that a set of three particular frequencies ω_{opt} leads to maximal pair creation. If this system is combined with the spatial force described in Sec. IV C leading to the optimal width $w_{opt}/c = 0.375$, we can construct the corresponding three i points. In Sec. V A we will show that these three i points can indeed provide excellent guidance with regard to the locations of the true optima.

Very similarly, the spatial variations presented by the amplitude led to the first three optimal values given by $V_{b,opt} = 0.733c^2$, $3.56c^2$, and $6.65c^2$. If this spatial force field is combined with the time-dependent force, we can construct a set of nine i points. In Sec. V B below we will show that even in this system each of the nine i points can provide good guidance with regard to the locations of the true optima.

A. Simultaneous optimization for the frequency and spatial width of the fields

In Fig. 7 we have graphed the first three optima for the space-time driven system, located at $\{\omega/c^2, Wc\} = \{0.8803, 0.3722\}$, $\{1.252, 0.3919\}$, and $\{2.482, 0.4232\}$. We

also show the corresponding elliptic contour plots in the immediate vicinity. The maxima are associated with Hessian indices given by $h = 0.1667$, 0.0047, and 0.00224, reflecting their various degrees of symbiosis. The corresponding relative orientation angles of the semimajor axes are $a = -8.57°$, $-3.54°$, and $-2.37°$.

Using the data obtained from the temporal- and spatial-only excitations derived in Secs. IV B and IV C, we can construct the corresponding three i points $\{\omega^{\{1,0\}}/c^2, W^{\{0,1\}}c\} = \{2.52, 0.375\}$, $\{1.26, 0.375\}$, and $\{0.844, 0.375\}$. Comparing them with the optima of the simultaneously excited system, we see that they can indeed provide excellent guidance with regard to the locations of the true optima.

In order to judge if the simultaneous presence of both forces can actually enhance the vacuum decay, we have also computed here the corresponding amplification factor, which we define here (similarly to the discussion in Sec. III E) as $N(T)^{\{1,1\}}/\max[N(T)^{\{1,0\}}, N(T)^{\{0,1\}}]$. As a reference, the number of created electron-positron pairs for the spatial force was $N(T)^{\{0,1\}} = 0.100$ (compare Fig. 5), while for the temporal excitation we measured $N(T)^{\{1,0\}} = 6.86 \times 10^{-3}$, 7.63×10^{-2}, and 3.47×10^{-1}, as shown in Fig. 4. If we determine the actual final particle yields for the vacuum decay under the simultaneous action, we find the corresponding amplification factors of 1.047, 1.323, and 0.95879. This suggests that - similarly to the case of the much simpler oscillator model- both forces cannot really mutually amplify the vacuum decay rate significantly. It certainly requires much more detailed and systematic studies to examine any general principles that would permit us to predict for which optimum one can achieve a largest amplification compared to the particle yields associated with the i points.

B. Simultaneous optimization for the frequency and spatial amplitude of the fields

To have a second and independent test of the generality of our findings, in this section we have optimized simultaneously the frequency of the time-dependent field together with the amplitude V_b of the spatial force field. Above we have examined for each temporal- and spatial-only system the first three optima. This leads to the prediction of the locations of nine i points. For better comparison, we present the nine coordinate pairs together with the true optima of the combined system in Table I.

Consistent with our prior findings, we also see here that each of the nine i points can provide again (remarkably accurate) guidance for the locations of the true optima.

Except for the i point associated with the pair $\{\omega, V_b\} = \{2.52c^2, 0, 733c^2\}$, we found that the average error, defined as $(\text{err}^{\{1,0\}} + \text{err}^{\{0,1\}})/2$, where $\text{err}^{\{1,0\}} \equiv (\omega^{\{1,1\}} - \omega^{\{1,0\}})/\omega^{\{1,1\}}$ and $\text{err}^{\{0,1\}} \equiv (V_b^{\{1,1\}} - V_b^{\{0,1\}})/V_b^{\{1,1\}}$ is usually significantly less than about 1%, suggesting also for this system the usefulness of the i points.

Finally, in Table II we have again examined the associated amplification factors. We find again only an insignificant amplification, which suggests that also here the temporally and spatially induced vacuum decay mechanisms are in competition with respect to each other. The only exception occurs for $\{\omega, V_b\} = \{2.52c^2, 0, 733c^2\}$, where already the i point

TABLE I. Comparison of the optimal frequency ω and spatial bump amplitude V_b with the coordinate pair of the corresponding i points $\omega^{\{1,0\}}$ and $V_b^{\{0,1\}}$. ($F_0 = 0.1c^3$, $T = 0.006$ a.u.; the electric field was chosen to be nonzero for the spatial domain $1.5/4 < x < 1.5/2$).

$\omega_L^{\{1,0\}}$	$\omega_L^{\{1,1\}}$	$V_b^{\{0,1\}}$	$V_b^{\{1,1\}}$	% Error	h Index	Angle α
0.838	0.851	0.733	0.729	1.0%	3.3×10^{-7}	0.2°
0.838	0.858	3.56	3.56	1.3%	8.9×10^{-4}	−1.8°
0.838	0.871	6.65	6.65	2.0%	3.7×10^{-4}	−1.5°
1.26	1.25	0.733	0.731	0.5%	1.1×10^{-5}	0.5°
1.26	1.26	3.56	3.56	0.2%	1.7×10^{-5}	0.1°
1.26	1.26	6.65	6.65	0.2%	9.1×10^{-5}	5.2°
2.52	2.52	0.733	0.524	14%	1.1×10^{-5}	0.01°
2.52	2.52	3.56	3.57	0.1%	7.2×10^{-2}	−0.6°
2.52	2.52	6.65	6.66	0.05%	6.2×10^{-2}	−0.7°

predicted the optimum with the largest error (14%). Here the amplification ($=1.76$) for the particle yield is actually largest. For a complete collection of the maxima locations, errors and h indices for all nine points, we refer the reader to Table I.

VI. SUMMARY AND OPEN QUESTIONS

In this work we have introduced the i-point methodology to analyze the location of optimal space-time parameters that maximize the physical output. As these i points reflect two independent dynamics, they can be obtained rather easily and can give guidance to the otherwise very complicated landscape in the parameter space. Such a method can potentially reduce the numerical complexity of the optimization algorithm. As a first proof of concept, we have initially considered a relatively simple model system to illustrate the mathematical concepts and then generalized these concepts to the more complicated dynamics of electron-positron pair creation from the vacuum. This serves as an example of a nontrivial system where it is of significant experimental interest to optimize simultaneously the spatial as well as temporal characteristics of the electromagnetic radiation pulse. Due to computational advances in the last few years it has become possible to optimize these characteristics under a solely spatial or temporal excitation. In this work, we have examined the concept of symbiotic optimization to permit us to examine the optimal characteristics of the combined action. We have shown that a

TABLE II. The corresponding average amplification factors $N(T)^{\{1,1\}}/\max[N(T)^{\{1,0\}}, N(T)^{\{0,1\}}]$ for each of the nine optima of Table I.

$\omega_L^{\{1,1\}}$	$V_b^{\{1,1\}}$	$N(T)^{\{1,1\}}$	Amplification
0.851	0.729	0.194897	0.9952
0.858	3.56	0.265196	0.9981
0.871	6.65	0.271256	0.9980
1.25	0.731	0.196363	1.0027
1.26	3.56	0.2664	1.0027
1.26	6.65	0.271963	1.0003
2.52	0.524	0.344704	1.7601
2.52	3.57	0.378513	1.4246
2.52	6.66	0.381796	1.4042

spatial amplitude optimization of the final number of created electron-positron pairs can be symbiotic or nonsymbiotic depending on the parameter regime. We have also generalized the concept of i points and showed that they can provide surprisingly reliable guidance for the optimal parameters of the systems that are excited by the combined action.

In order to provide a few systematic steps towards this difficult optimization problem, we have parametrized each field by only a single spatial and temporal parameter. The question, of course, arises if and how the basic conclusion about the Hessian index and the usefulness of the computationally much easier i points as guidance for the location of the true maxima can be generalized to higher-dimensional optimization schemes. For example, if the spatial field were to be parametrized simultaneously by N parameters with s_j (spatial extension, amplitudes, etc.), and similarly the temporal field by M parameters with t_j, then corresponding hyperellipsoids around the optimal $(N + M)$ parameters in this $(N + M)$ dimensional space could also be characterized by a generalized Hessian index. It would generalize to $h \equiv \Sigma_{i,j}[\partial^2 F/(\partial t_i \partial s_j)]^2/\{\Sigma_i[\partial^2 F/(\partial t_i \partial t_i)]\Sigma_i[\partial^2 F/(\partial s_i \partial s_i)]\}$, which reduces naturally to our original Hessian index $h = [\partial^2 F/(\partial t_1 \partial s_1)]^2/\{[\partial^2 F/(\partial t_1 \partial t_1)][\partial^2 F/(\partial s_1 \partial s_1)]\}$ for $N = M = 1$. In the ideal (and hopefully) future case, where we can permit an infinite-dimensional optimization for the spatial as well as temporal degrees, the i points would become two-component i functions, but their basic role in predicting the locations of the optima of the simultaneous action should remain the same as discussed here.

While for the geometrical configurations examined in this work, the tunneling and multiphoton-based pair-creation mechanisms seem almost to be in competition with each other, for other scenarios, such as the so-called dynamically assisted Schwinger effect [51,52], both fields can mutually help each other to increase the yield. The more competitive behavior observed for our system might also be a consequence of the fact that we focused our comparison to those cases where each individual force was already optimized by itself, leading to the i points.

We should conclude this outlook with a critical comment about the physical realizability of optimal space-time profiles of electromagnetic-field configurations. While the focus of this work has been on the optimization of the quantum field theoretical dynamical response of the vacuum state, one should not forget that any experimentally realizable configurations in three dimensions have also to satisfy the confines of the Maxwell equations and cannot be manipulated at will. These would intimately relate the possible spatial and temporal variations of the fields. We should therefore point out that it would be an interesting and important future challenge to construct fields that can even meet the physical boundary conditions provided by Maxwell's theory.

[1] For a recent review, see, B. S. Xie, Z. L. Li, and S. Tang, Matter Radiat. Extremes **2**, 225 (2017).

[2] For a comprehensive review, see A. Di Piazza, C. Müller, K. Z. Hatsagortsyan, and C. H. Keitel, Rev. Mod. Phys. **84**, 1177 (2012).

[3] For recent advances, see, e.g., https://eli-laser.eu/.

[4] J. S. Schwinger, Phys. Rev. **128**, 2425 (1962).

[5] W. Greiner, B. Müller, and J. Rafelski, *Quantum Electrodynamics of Strong Fields* (Springer-Verlag, Berlin, 1985).

[6] S. R. Coleman, Nucl. Phys. B **298**, 178 (1988).

[7] For early work, see G. Breit and J. A. Wheeler, Phys. Rev. **46**, 1087 (1934).

[8] H. R. Reiss, J. Math. Phys. **3**, 59 (1962); Phys. Rev. Lett. **26**, 1072 (1971).

[9] E. S. Fradkin, D. M. Gitman, and Sh. M. Shvartsman, *Quantum Electrodynamics with Unstable Vacuum* (Springer-Verlag, Berlin, 1991).

[10] A. A. Grib, S. G. Mamaev, and V. M. Mostepanenko, *Vacuum Quantum Effects in Strong Fields* (Atomizdat, Moscow, 1988) (republished by Friedmann Laboratory, St. Petersburg, Russia, 1994).

[11] N. B. Narozhny and A. I. Nikishov, Sov. J. Nucl. Phys. **11**, 596 (1970).

[12] E. Brezin and C. Itzykson, Phys. Rev. D **2**, 1191 (1970).

[13] V. S. Popov, JETP Lett. **13**, 185 (1971); Sov. Phys. JETP **34**, 709 (1972).

[14] W. Y. Wu, F. He, R. Grobe, and Q. Su, J. Opt. Soc. Am. B **32**, 2009 (2015).

[15] C. Kohlfürst, Master's thesis, Graz University, arXiv:1212.0880.

[16] C. Kohlfürst, M. Mitter, G. von Winckel, F. Hebenstreit, and R. Alkofer, Phys. Rev. D **88**, 045028 (2013).

[17] F. Hebenstreit and F. Fillion-Gourdeau, Phys. Lett. B **739**, 189 (2014).

[18] S. S. Bulanov, C. B. Schroeder, E. Esarey, and W. P. Leemans, Phys. Plasma **19**, 093112 (2012).

[19] S. S. Dong, M. Chen, Q. Su, and R. Grobe, Phys. Rev. A **96**, 032120 (2017).

[20] J. Unger, S. S. Dong, R. Flores, Q. Su, and R. Grobe, Phys. Rev. A **99**, 022128 (2019).

[21] J. Unger, S. S. Dong, Q. Su, and R. Grobe, Phys. Rev. A **100**, 012518 (2019).

[22] F. Hund, Z. Phys. **117**, 1 (1941).

[23] A. Hansen and F. Ravndal, Phys. Scr. **23**, 1036 (1981); N. Dombey, and A. Calogeracos, Phys. Rep. **315**, 41 (1999).

[24] R. E. Wagner, M. R. Ware, Q. Su, and R. Grobe, Phys. Rev. A **81**, 052104 (2010).

[25] W. Su, M. Jiang, Z. Q. Lv, Y. J. Li, Z. M. Sheng, R. Grobe, and Q. Su, Phys. Rev. A **86**, 013422 (2012).

[26] F. Fillion-Gourdeau, E. Lorin, and A. D. Bandrauk, Phys. Rev. Lett. **110**, 013002 (2013).

[27] Q. Z. Lv, S. Dong, C. Lisowski, R. Pelphrey, Y. T. Li, Q. Su, and R. Grobe, Phys. Rev. A **97**, 053416 (2018).

[28] S. Schmidt, D. Blaschke, G. Röpke, S. A. Smolyansky, A. V. Prozorkevich, and V. D. Toneev, Int. J. Mod. Phys. E **7**, 709 (1998).

[29] Y. Kluger, E. Mottola, and J. M. Eisenberg, Phys. Rev. D **58**, 125015 (1998).

[30] J. C. R. Bloch, V. A. Mizerny, A. V. Prozorkevich, C. D. Roberts, S. M. Schmidt, S. A. Smolyansky, and D. V. Vinnik, Phys. Rev. D **60**, 116011 (1999).

[31] R. Alkofer, M. B. Hecht, C. D. Roberts, S. M. Schmidt, and D. V. Vinnik, Phys. Rev. Lett. **87**, 193902 (2001).

[32] G. R. Mocken, M. Ruf, C. Müller, and C. H. Keitel, Phys. Rev. A **81**, 022122 (2010).

[33] A. M. Fedotov, E. G. Gelfer, K. Y. Korolev, and S. A. Smolyansky, Phys. Rev. D **83**, 025011 (2011).

[34] J. Unger, S. S. Dong, R. Flores, Q. Su, and R. Grobe, Las. Phys. **29**, 065302 (2019).

[35] D. E. Kirk, *Optimal Control Theory: An Introduction* (Prentice-Hall, Englewood Cliffs, NJ, 1970).

[36] R. Dechter, *Constraint Processing* (Morgan Kaufmann, San Francisco, 2003).

[37] D. S. Naidu, *Optimal Control Systems* (CRC Press, Baca Raton, FL, 2003).

[38] J. J. Leader, *Numerical Analysis and Scientific Computation* (Addison Wesley, Reading, MA, 2004).

[39] R. Battiti, M. Brunato, and F. Mascia, *Reactive Search and Intelligent Optimization* (Springer-Verlag, Heidelberg, 2008).

[40] W. Sun and Y. X. Yuan, *Optimization Theory and Methods: Nonlinear Programming* (Springer-Verlag, Heidelberg, 2010).

[41] A. Gosavi, *Simulation-Based Optimization* (Springer-Verlag, Heidelberg, 2015).

[42] D. Bertsekas, *Dynamic Programming and Optimal Control* (Athena Scientific, Belmont, MA, 2017).

[43] For an early review, see, e.g., T. Cheng, Q. Su, and R. Grobe, Contemp. Phys. **51**, 315 (2010).

[44] M. D. Feit, J. A. Fleck, Jr., and A. Steiger, J. Comput. Phys. **47**, 412 (1982).

[45] A. D. Bandrauk and H. Shen, J. Chem. Phys. **99**, 1185 (1993).

[46] J. W. Braun, Q. Su, and R. Grobe, Phys. Rev. A **59**, 604 (1999).

[47] P. Krekora, Q. Su, and R. Grobe, Phys. Rev. A **73**, 022114 (2006).

[48] F. Sauter, Z. Phys. **69**, 742 (1931).

[49] T. Cheng, M. R. Ware, Q. Su, and R. Grobe, Phys. Rev. A **80**, 062105 (2009).

[50] Q. Z. Lv, Q. Su, and R. Grobe, Phys. Rev. Lett **121**, 183606 (2018).

[51] R. Schützhold, H. Gies, and G. Dunne, Phys. Rev. Lett. **101**, 130404 (2008).

[52] G. V. Dunne, H. Gies, and R. Schützhold, Phys. Rev. D **80**, 111301(R) (2009).